

SEISMICITY, GROUNDWATER LEVEL VARIATIONS AND EARTH TIDES IN THE HRONOV-POŘÍČÍ FAULT ZONE, CZECH REPUBLIC

Petr KOLÍNSKÝ *, Jan VALENTA and Renata GAŽDOVÁ

*Institute of Rock Structure and Mechanics, Academy of Sciences of the Czech Republic, v.v.i.,
V Holešovičkách 41, 182 09 Prague, Czech Republic*

**Corresponding author's e-mail: kolinsky@irms.cas.cz*

(Received January 2012, accepted June 2012)

ABSTRACT

Local seismicity of the Hronov-Poříčí Fault Zone is studied using two-year continuous seismic data from four seismic stations in the area. Newly developed software for automatic seismic events detection is introduced – it is based on the method used at the Icelandic seismic network. Twelve major local earthquakes are detected, localized and their magnitudes are estimated. Simultaneously, groundwater levels are continuously monitored in three wells in the area. Multiple-filtering method, originally used for processing of broadband and dispersed seismic signals, is modified and used for the frequency-time analysis of the water level data. Dominant tidal influence on the groundwater level variations is shown. Theoretical tidal potential for all three well locations is computed. Groundwater data and tidal potential are bandpass filtered to focus on the semidiurnal periods. Mutual amplitude ratio and phase shift between both quantities are computed. Each of the three wells exhibits different pattern of the groundwater level variations with respect to tides. A distinct change in the phase shift is observed at the VS-3 well in the second half of 2009. In the same time span, increased seismic activity is also observed. However, other two wells do not exhibit any evidence of such phase shift. Detailed groundwater level data analysis does not prove any significant rises or drops of the groundwater levels in 28 day intervals around the detected local events. In contrast, unexplained groundwater level drop in the V-34 well is observed 18 hours before the teleseismic Tohoku earthquake, Japan, March 11, 2011, $M_w = 9.0$.

KEYWORDS: Eastern Bohemian Massif, groundwater level, seismicity, earth tides, air pressure

1. INTRODUCTION

The Bohemian Massif – the Central European Variscan structure – is an area with weak intraplate seismicity. Only its marginal parts are affected by young – up to Early Quaternary – tectonic movements responsible for uplift of mountain chains on the borders. These marginal parts are connected with the most seismoactive zones of the Bohemian Massif. The most seismically active is the West Bohemia/Vogtland zone. The second most active area is situated on the NE margin of the Bohemian Massif. It is approximately 40–60 km wide and 150 km long and comprises a number of NW-SE and NNW-SSE-striking faults. This zone forms a SE termination of the important central European tectonic structure – the Elbe Fault system (see e.g. Špaček et al., 2006). The targeted area of the Hronov-Poříčí Fault Zone (HPFZ) belongs to this seismoactive zone.

The HPFZ is a result of complicated and long-lasting evolution since the late Paleozoic. It comprises a system of fractures – a dominant reverse fault (thrust) and accompanying parallel or oblique dislocations. Along the main fault the NE block was relatively uplifted. The NW-SE striking HPFZ is approximately 40 km long and up to 500 m wide. More detailed description of the tectonic evolution can be found e.g. in the paper by Valenta et al. (2008).

The relatively frequent local seismic activity of the HPFZ is a proof of a present-day mobility. The depths of local earthquakes are mostly between 5 and 15 km (Schenk et al., 1989). The strongest historical earthquake occurred in 1901 (Woldřich, 1901) and reached the magnitude of approx. 4.6. References and overview of the historical earthquakes are mentioned in the papers by Málek et al. (2008) and Stejskal et al. (2007). Another proof of the HPFZ mobility is the presence of CO₂-rich mineral springs in the area. The springs belong to a larger zone extending to Poland.

This paper is based on seismic, hydrological and meteorological data observed in the area of the HPFZ. Several deep wells are located in the area of the HPFZ and groundwater level has been measured in some of them for years (Stejskal et al., 2007). A new detailed research focused on the hydrological effects of seismicity has been described within this paper.

The groundwater level is affected mainly by hydrological, meteorological and artificial factors. Moreover, the level is also influenced by deformation processes in the Earth's crust including tidal forces and changes in stresses resulting from tectonic activity. The stress variations can cause pre-, co- and post-seismic groundwater level changes. The pre-seismic changes play the most important role as they can represent possible earthquake precursors.

Table 1 Seismic stations, their location and other parameters.

station name	code	longitude [°N]	latitude [°E]	Altitude [m]	sensor	equipment	sampling [Hz]
Chvaleč	CHVC	16.0547	50.5881	600	STS-2	RUP	250
Dobruška / Polom	DPC	16.3222	50.3502	748	STS-1	Q330HR	100
Ostaš	OSTC	16.2156	50.5565	556	CMG-40T	RUP	250
Úpice	UPC	16.0121	50.5074	416	S5-S / STS-2	Q330S	100

An overview of the literature describing effects of earthquakes on hydrogeological structures from various seismo-active regions and reporting the characteristics of pre-seismic groundwater level changes, such as the size of the anomaly, lead time of the occurrence and relations between the earthquake magnitude or epicentral distance and the amplitude of the anomaly, is given by Gaždová et al. (2011).

Stejskal et al. (2007) studied two-year time series of groundwater level data and their connection with seismicity of the given area. They used five wells – three of them are also used in our study. They decomposed the water level data into barometric response, diurnal and semidiurnal tidal responses and low- and high-frequency components. Two pre-seismic steps in one of the wells were found for local earthquakes which occurred in 2005. Málek et al. (2008) detected several local earthquakes from 2005 to 2007 with a swarm-like set of events in August 2007. Other studies in the last years concerned also geomorphological research (Stejskal et al., 2006) and geoelectrical profiling (Valenta et al., 2008).

The present paper continues with the research in the HPFZ. To study the relationship between groundwater level changes and seismic events is the key point of this study. We directly follow the research taken by Stejskal et al. (2007 and 2009) and Málek et al. (2008). Our groundwater level data represent the observations in three wells from October 2008 to July 2011. Air pressure and precipitation data from the area of interest are also used. Seismic measurement was enhanced by the deployment of a new seismic station Chvaleč (CHVC) in 2009. We use continuous seismic data from July 2009 up to June 2011 measured at four stations in this study. In addition to the previous papers, not only new data series are studied, but also frequency-time analysis and bandpass filtering of the groundwater data are implemented in the simultaneous analysis with theoretical Earth tidal potential computed for respective wells.

2. DATA

2.1. SEISMIC STATIONS

Two seismic stations, Ostaš (OSTC) and Chvaleč (CHVC), are operated by the Institute of Rock Structure and Mechanics, Academy of Sciences of the Czech Republic (ASCR), in the area of the

HPFZ. In addition, two other stations, Dobruška-Polom (DPC) and Úpice (UPC), operated by the Institute of Geophysics, ASCR are located nearby (e.g. Zedník and Pazdírková, 2010). The latter two stations are also part of the Czech Regional Seismic Network (CRSN). All four stations are situated around the area of interest, see Figure 1. Stations DPC and UPC have been measuring since 1992 and 1983, respectively. In 2010, the sensor at UPC was changed to broadband. The station OSTC was installed in October 2005 and the station CHVC in May 2009 with the aim to cover the HPFZ for a better location of weak seismic events.

For processing, we selected the time period of two years when all four stations were in operation. It means from July 2009 until April 2011 when the latest data were harvested. All four stations are processed together as a local network while detecting and locating weak earthquakes. Station OSTC also works as a small-aperture array. It consists of the central broadband sensor and three satellite three-component shortperiod sensors (Málek et al., 2008). In this study, only the central broadband sensor is used for data processing. All four stations are equipped with broadband seismometers with sampling frequency 100 or 250 Hz, see Table 1. Stations OSTC and CHVC use the RUP acquisition system (Brož and Štrunc, 2011).

2.2. HYDROLOGICAL WELLS

Hydrological observations are carried out by the Institute of Rock Structure and Mechanics, ASCR, in three boreholes: Adršpach (VS-3), Teplice (V-34) and Třtice (HJ-2) by water-level meters, see Table 2. Part of the data from the VS-3 well is provided by the T. G. Masaryk Water Research Institute. The water level measurement is based on the difference of the free air pressure above the water and the hydrostatic pressure below the water table. The differential pressure is measured by DCP-PLI03 pressure sensors. The sensors are connected to digital data loggers with a capacity of 32 000 measured values. The data are recorded with a sampling interval of 10 minutes. The accuracy of the measurement is 0.1 % using the immersion depth of 10 m and resolution is 1 mm. The recorded data are downloaded using a laptop linked with a RS232 serial port.

The VS-3 well is drilled in the valley of the Metuje River. It taps aquifers in the Upper Cretaceous

Table 2 Monitored wells and their parameters.

well name	code	longitude [°E]	latitude [°N]	altitude [m]	depth [m]	Average groundwater level depth [m]
Adršpach	VS-3	16.1414	50.6114	486	305	3
Teplice	V-34	16.1665	50.5840	523	281	124
Trtice	HJ-2	16.0832	50.4261	309	35	1

sediments (Middle Turonian to Cenomanian sandstones, marlstones and silicites). It is opened at depths of 38-207 m and 217-260 m. The V-34 well is drilled near the town of Teplice nad Metují. The well taps aquifer in the Upper Cretaceous sediments (Cenomanian sandstones) and is opened at depth of 238-281 m. The HJ-2 well is situated near the system of fractures at the Upper Cretaceous sediments. CO₂ rich mineral water spring is located approximately 600 m from the well. The HJ-2 well is the shallowest of the three monitored wells and its hydraulic connection with the surface spring was proved earlier. For details, see Stejskal et al. (2007). All three wells are located in the distance of 8 to 10 km from the HPFZ. The HJ-2 well lies south of the fault and VS-3 and V-34 wells are north of it, see Figure 1.

For the processing, we selected the period from November 2008 to June 2011, i.e. two years and eight months. This time period is broader than the one used for the seismic data (starting from July 2009). Due to the technical reasons, wells V-34 and HJ-2 have gaps in data in the middle of the time period of interest. Data are missing from July 22, 2009 to March 27, 2010 for the V-34 well and from December 6, 2009 to February 12, 2010 for the HJ-2 well.

In addition to the groundwater levels, air-pressure was measured at the OSTC seismic station by the Institute of Rock Structure and Mechanics, ASCR. The air pressure sensor is placed in the underground of the seismic station avoiding the fluctuations caused by the wind. Precipitation data from the meteorological station near the VS-3 well were provided by the Czech Hydrometeorological Institute.

3. DETECTION AND LOCATION OF SEISMIC EVENTS

The seismic data are recorded at four seismic stations. The data are continuous and the sampling frequency was initially set to 100 Hz at all stations. On December 9, 2009 the CHVC station was set to 250 Hz sampling and later on (February 26, 2011) also the OSTC station was set to this sampling frequency.

Two years of continuous data from four stations could not be easily processed by hand and certain amount of automated processing is necessary. We are mostly interested in automatic detection of possible local events. For solving this task, we have found an inspiration in the South Icelandic Lowland (SIL) data acquisition system (Stefánsson et al., 1993; Jakobsdóttir et al., 2002).

The SIL event detector uses comparison of amplitudes in two adjacent windows of the seismic trace – an approach similar to the Short Time Average / Long Time Average (STA/LTA). The difference is that both windows have the same length. We have adopted this concept and modified it in order to be sensitive for local events and ignore the teleseismic ones.

The seismic data are frequency filtered to remove the far long-period events and a high-frequency noise. Bandpass filter removing frequencies below 5 Hz and above 30 Hz is used. Amplitudes in two adjacent windows are compared. The length of the windows essentially determines a type of events to be detected. The longer the windows, the farther events (longer periods) are detected. For local earthquake detection, we have found the optimal length of windows to be 0.4 s. The length of both windows is the same. If a ratio of both windows exceeds certain threshold then the possible local event is reported. Also possible P- and S-phases are determined based on the amplitude ratio between the vertical and horizontal components.

Described processing steps select about ten thousand possible local events per month for every station. This amount is still impractical to be sorted by hand and hence another automatic processing step is necessary. In this step we look at a coincidence of candidate events in time at more stations.

The local events should be observed within a certain time window on several stations. The size of the time window can be estimated considering station distance and velocity of seismic waves. The maximal length of the time window within which the event must be detected on two stations equals the station distance divided by the velocity of P- or S-waves. This holds for the limiting case, when the event is located on the profile delineated by the two stations at a zero depth. For all other cases the time window is shorter.

Hence, the third step is a selection of candidates according to their arrival times. Such selection reduces the number of candidates to about twenty or thirty per month, which is a reasonable number for a manual inspection.

The final step is then a manual inspection of detected events, mainly rejection of quarry blasts. Twelve local seismic events are detected for the time interval from July 2009 to April 2011 with local magnitude up to $M_L = 1.5$. An example of one of the event records at all four stations is given in Figure 2 for all three components.

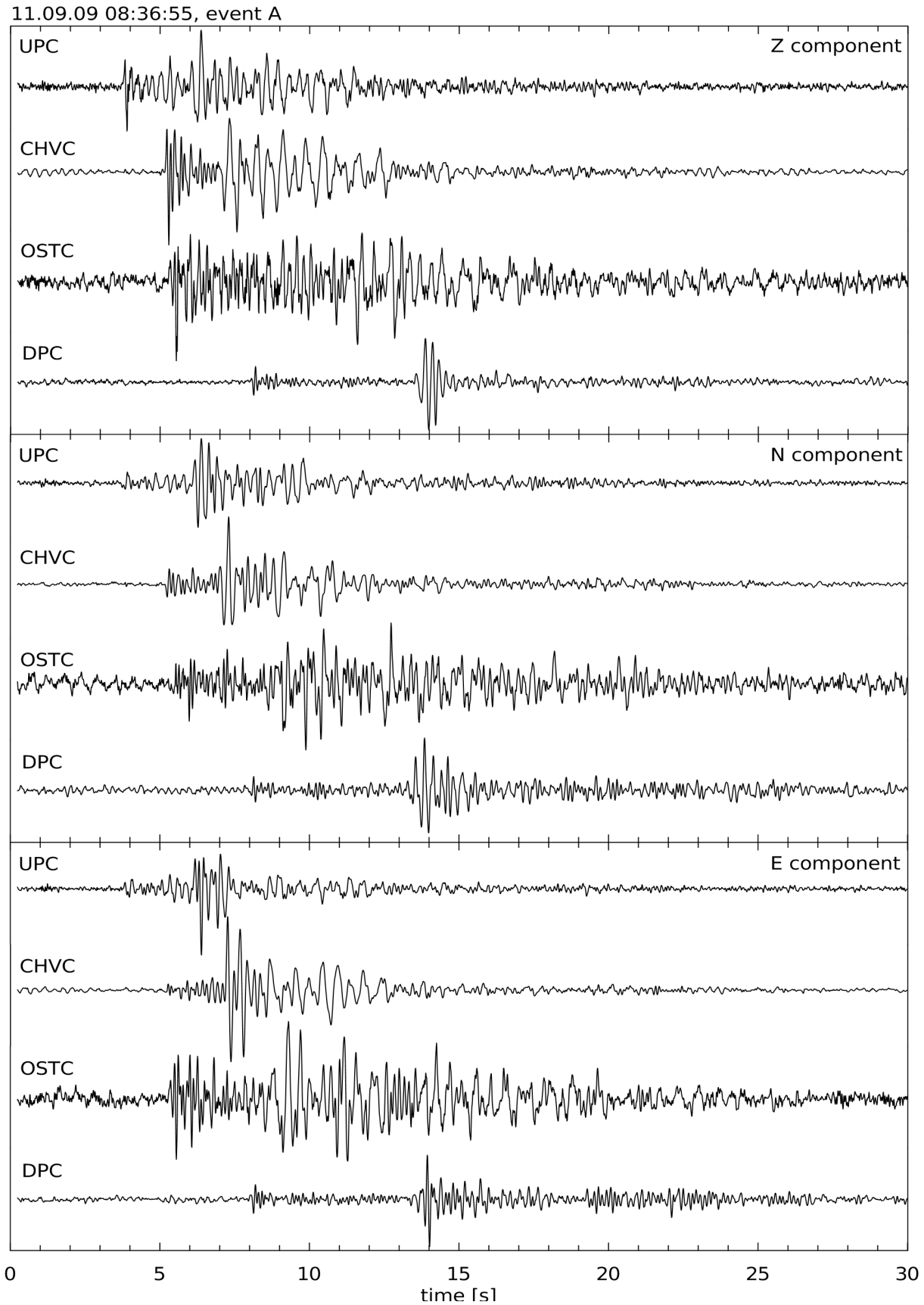


Fig. 2 An example of the event A from September 11, 2009, origin time 08:36:55, is shown. Records at all four local stations and all three components are presented. The records are bandpass filtered between 5 and 30 Hz. For each component, the records are ordered according to their epicentral distances.

Table 3 Detected and located earthquakes with estimated local magnitudes. “ M_L ” column shows the magnitudes estimated in our study. “ M_L CRSN” column shows the local magnitudes estimated by the Czech Regional Seismic Network. The column labeled “operating wells” reads, how many wells were operating in the time of the event. Last column of the table indicates four events, for which the details of groundwater levels are plotted in Figure 5.

date	origin time [UTC]	label	longitude [°E]	latitude [°N]	depth [km]	M_L	M_L CRSN	operating wells	details
11 09 2009	08:36:56.58	A	16.0159	50.5369	8.0	0.3		2	Fig. 5
11 09 2009	15:39:16.79	B	16.1043	50.5193	13.1	0.8	0.8	2	Fig. 5
30 09 2009	08:30:24.61	C	15.9711	50.3270	not est.	1.1		2	
08 10 2009	08:01:40.28	D	15.9811	50.3278	not est.	1.5		2	
24 10 2009	13:06:09.25	E	16.1077	50.5210	12.7	0.6	0.6	2	
04 01 2010	12:03:47.16	F	16.5088	50.5277	16.5	1.0	1.0	1	
05 01 2010	03:33:33.44	G	16.1084	50.5201	12.7	0.2		1	
24 01 2010	13:32:49.98	H	16.3356	50.4410	14.8	0.1	0.6	1	
28 01 2010	19:21:17.56	J	16.1063	50.5220	10.2	0.1		1	
16 02 2010	18:22:53.88	K	16.4135	50.2461	23.5	0.8	not est.	2	
29 12 2010	16:45:51.68	L	16.2709	50.4832	8.3	0.6	0.7	3	Fig. 5
17 01 2011	06:18:30.22	M	16.0493	50.4499	12.0	0.7		3	Fig. 5

Table 4 Located quarry blasts and their location error. All distances are in kilometers, all azimuths are in degrees. “Epic dist” is a distance of the location of the blast to the centroid of the network, “quarry dist” is a distance of the real quarry to the same center of the network and “diff dist” is the difference of the distances. The same applies for the backazimuths. “Total dist diff” is the distance between the event location and the real blast.

date	origin time	longitude [°E]	latitude [°N]	M_L	epic dist	quarry dist	diff dist	epic az	quarry az	diff az	total dist diff
08 10 2010	12:11:23.45	16.2766	50.7099	2.1	24.92	22.79	2.13	62.7	61.9	0.8	2.16
12 10 2010	09:37:32.41	16.4009	50.6279	2.1	22.66	22.70	0.05	32.3	29.3	3.0	1.18
12 10 2010	12:09:42.46	16.3626	50.6279	2.6	20.44	20.24	0.21	36.5	33.1	3.4	1.22
25 10 2010	08:05:18.24	16.2970	50.6895	2.1	23.41	22.79	0.62	57.4	61.9	4.5	1.93

We do not consider this set of events to represent a complete catalogue of the area in the given time period. The major limitation is given by the fact that we select only the events which are detected at least by three stations. Small events detected by lower number of stations are not considered in our study. This approach, however, allows us to select few major events which are of the most importance for this study as the groundwater level variations are assumed to be more pronounced in relation with larger earthquakes.

The selected events, see Table 3, are then located, see Figure 3. The location, based on P- and S-wave arrivals, is done for a homogeneous velocity model with velocities of P-waves 5.320 km/s and S-waves 3.205 km/s. The location error is estimated using records of quarry blasts. The blasts are processed exactly in the same manner as local events and the resulting locations are compared with known locations of the quarries where the blasts were fired, see Table 4.

The active quarries were, unfortunately, located only outside the network, approximately 15 km from

the nearest seismic station, see pentagrams in Figure 3. The location error for quarry blasts is about two kilometers in the worst case, see Table 4. However, the location error inside the network is assumed to be smaller. On the other hand, blasts were fired at the Earth surface and hence we benchmarked only the uppermost crust velocities by this approach.

Local magnitude M_L is estimated for each of the events. A traditional formula (used for example at WEBNET, see Fischer et al., 2010)

$$M_L = \log A_z + k_1 \cdot \log R + k_2$$

is used. A_z is the highest amplitude of the vertical component in $\mu\text{m/s}$, both logarithms are decimal. R is the hypocentral distance in km. Constant k_1 , which adjust the dependence on the distance, is given as a slope of the dependence of the maximal amplitude on the distance for four stations and ten events. Two events (C and D) were omitted since their depth estimation was uncertain. Because the forty points in the $[\log A_z / \log R]$ plane are still very scattered, we

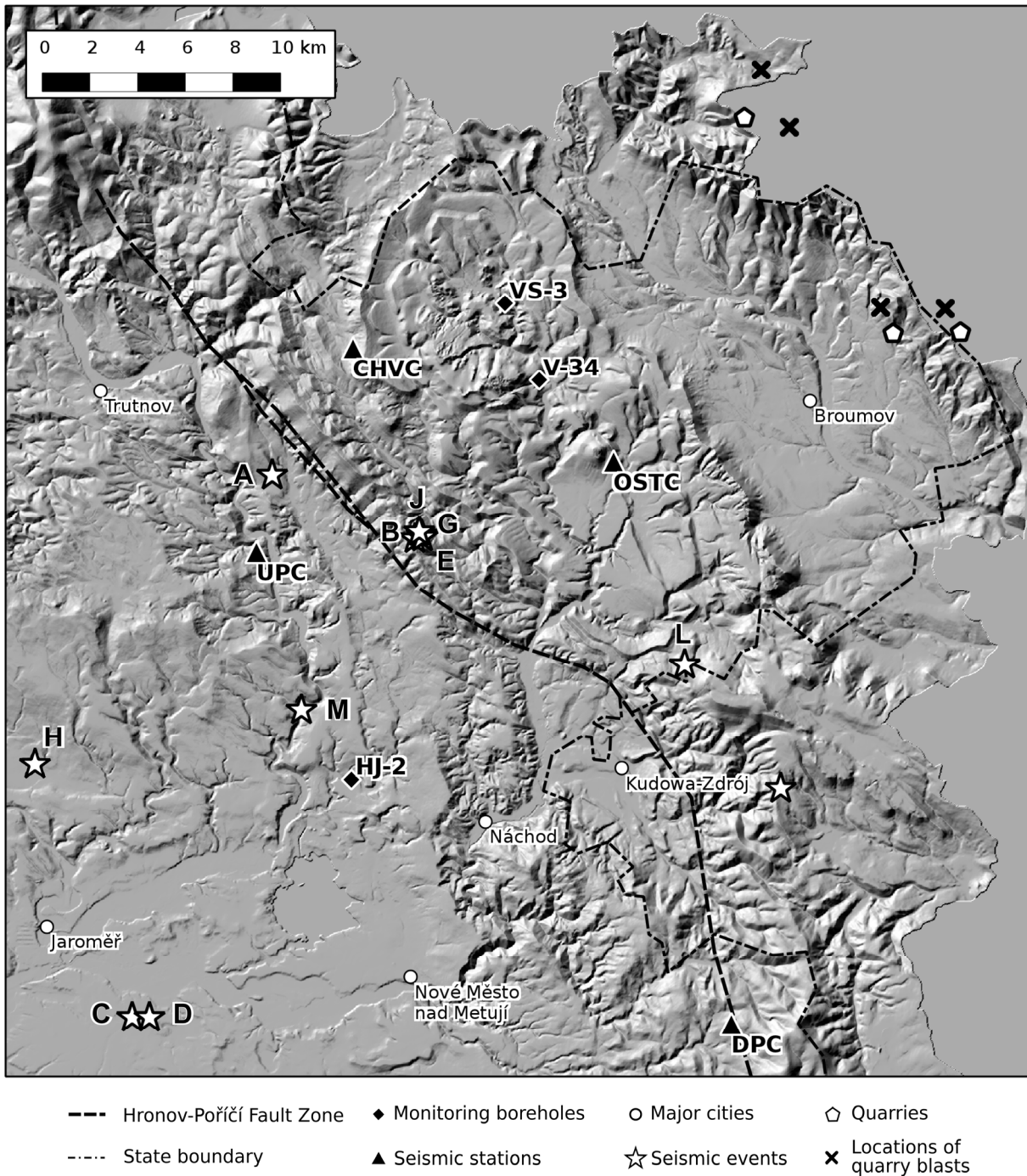


Fig. 3 Topographic map of the HPFZ area with seismic stations and wells. Dashed line represents the Hronov-Poříčí Fault Zone. Asterisks denote locations of detected earthquakes (event F is located out of the map east from OSTC station and event K is south of the DPC station) and crosses are locations of quarry blasts. The distance of these blast locations from the actual quarries (pentagons) allows to estimate the location error, see text for detailed explanation.

further decided to omit outliers what yielded the constant to be $k_1 = 2.29$. Constant $k_2 = -2.14$ adjusts the whole magnitude scale to the previously determined magnitudes from the CRSN. Resulted local magnitudes are given in Table 3. We see that four of the five magnitudes estimated by CRSN (B, E, F and L) are matched by our determination of M_L .

4. GROUNDWATER AND TIDES

Usual processing of the groundwater data concerns not only the water level data itself, but other factors influencing the water level are also taken into account. In the area of interest, air pressure was measured at the seismic station OSTC, precipitation data were provided from the meteorological station

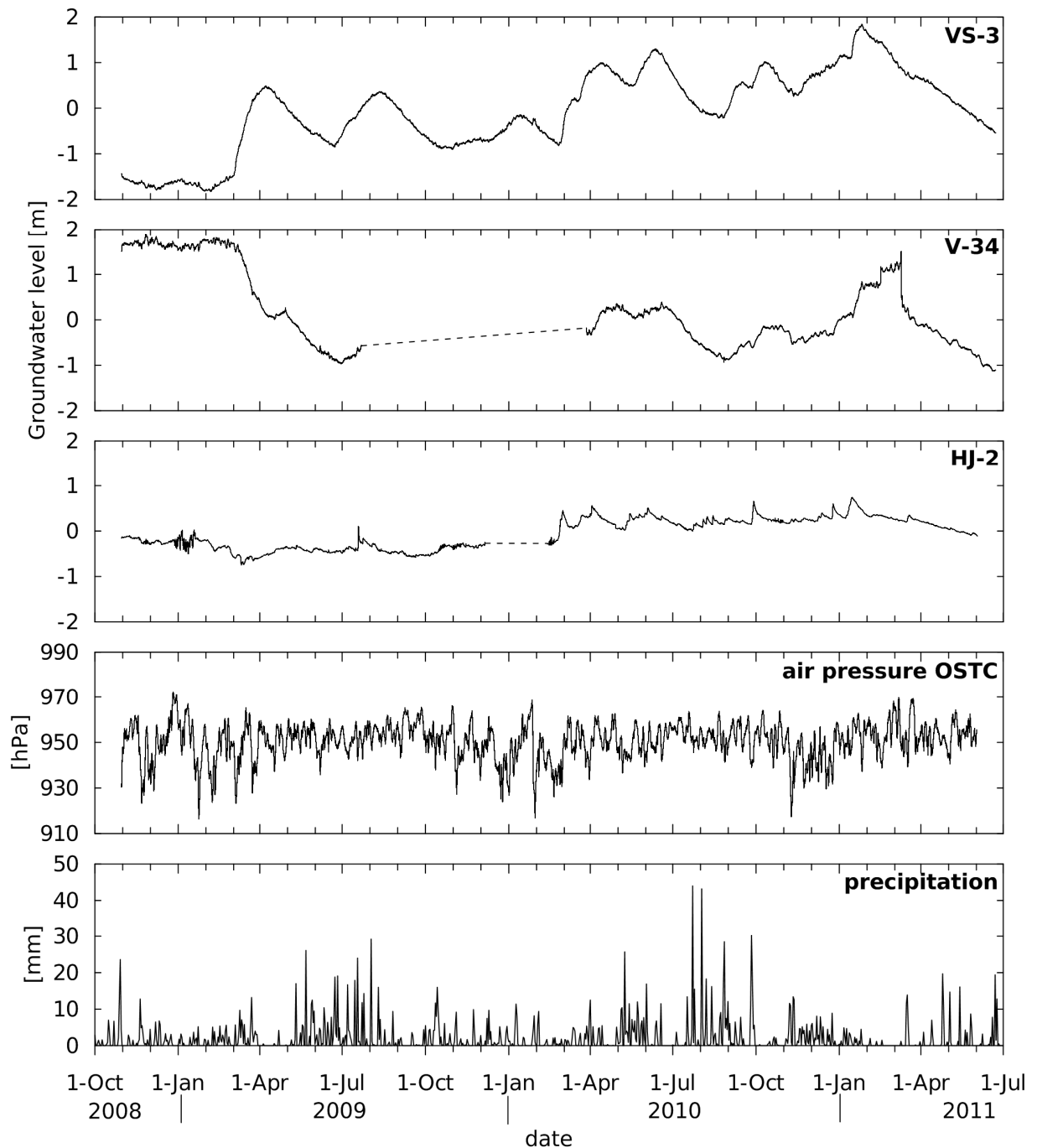


Fig. 4 Groundwater levels for all three wells, air pressure and precipitation for the time period of interest.

Adršpach (in operation by the Czech Hydro-meteorological Institute). Theoretical tides were computed for all three well locations using software developed by Wenzel (1993) and modified by Skalský (1991). The global tidal model of an ellipsoidal rotating, elastic Earth “Wahr-Dehant-Zschau” was used, see Wahr (1981), Dehant (1987) and Zschau and Wang (1981). Tidal potential is used for this study. Measured groundwater levels for all three wells as

well as air pressure and precipitation data are shown in Figure 4.

We do not provide decomposition of the groundwater level data into air pressure, tidal, low and high frequency components in the present study in a way it was done by Stejskal et al. (2007 and 2009). Instead, we focus on short-period abrupt changes in the water level data which may coincide with local seismic events and we provide a frequency-time

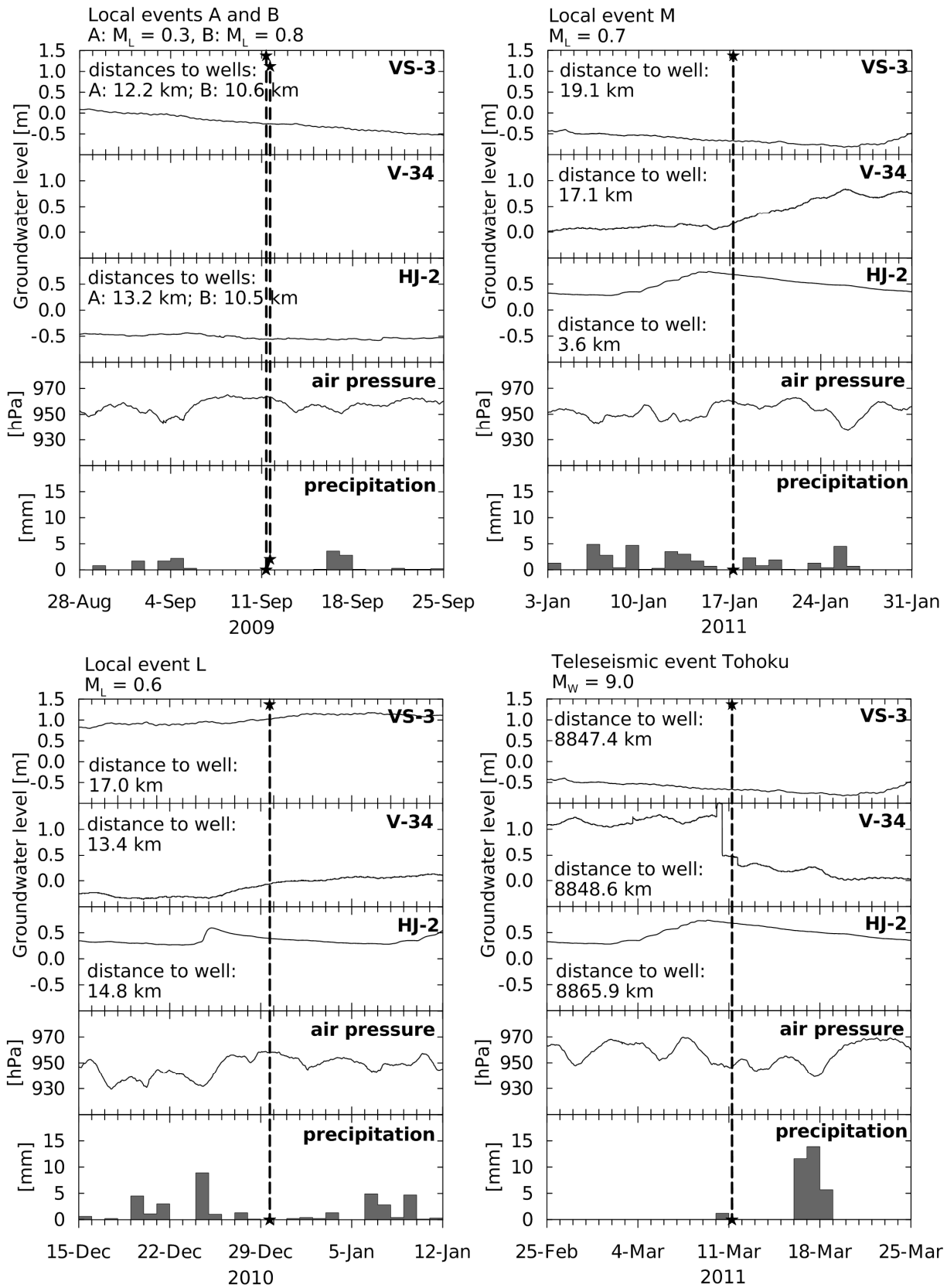


Fig. 5 Courses of groundwater levels, air pressure and precipitation in the period of 14 days before and after four local and one teleseismic events are shown.

analysis of a broad spectrum of periods. We also study the amplitude ratio and phase shifts between the bandpass filtered water level and theoretical tides as tides are the quantity which influences the groundwater level the most. The changes in the phase delay of the water level after the tides may indicate changes in the stress conditions of the rock massifs. In case of an abrupt change of the water level, precipitation and air pressure data are used to check if the water level step does or does not coincide with a similar abrupt change in both meteorological quantities.

Groundwater level data are processed in the following three ways:

1. Visual inspection of 14 days before and after local seismic events to find out any suspicious water level rises or drops.
2. Frequency-time analysis of the whole time series in order to understand the groundwater level behavior itself.
3. Joint analysis of measured groundwater and theoretical tidal time series to determine amplitude ratio and phase shift between the quantities.

4.1. VISUAL INSPECTION

A time window of 14 days before and 14 days after each of the detected local seismic event origin times is taken and any distinct water level changes are searched. The motivation for this approach is based on the study of Stejskal et al. (2009) who recorded two groundwater pre-seismic steps at VS-3 well before August 10, 2005 and October 25, 2005, earthquakes. We inspect all twelve events detected from 2009 to 2011. Figure 5 shows four local events (A, B, L and M, for their location see Figure 3) with corresponding time series of water level data for all three wells. Although the events in Figure 5 are selected so that they are located at the HPFZ or in the close vicinity of the wells, we do not find any remarkable drops or rises of the water levels in the given time period.

Further, an opposite approach is used. We look at the significant groundwater level steps and search if any teleseismic or regional event occurred close to these steps in time. As an unusual phenomenon during the 32 months time series, we consider drop of 95 cm recorded at the V-34 well, see right bottom plot in Figure 5, which occurred between 11:30 and 11:40 on March 10, 2011, what is 18 hours before the M_w 9.0 Tohoku earthquake, Japan, March 11, 2011, origin time 05:46:24. Air pressure and precipitation data do not exhibit any significant unusual behavior close to the distinct groundwater step.

4.2. FREQUENCY-TIME ANALYSIS

Analysis covering a broad spectrum of the groundwater level time series substitutes the traditional splitting of the data into low and high frequency components, as used, for example, in studies by Stejskal et al. (2007, 2009). Filtering the

spectrum on many frequencies allows studying the different influences controlling the groundwater level in detail. As tidal effects are the most prominent ones, filters are centered to correspond to the principal tidal frequencies.

Spectra of groundwater level (VS-3), theoretical tide potential (VS-3) and air pressure (OSTC) are plotted in Figure 6. All three spectra are computed using the whole 32 months duration of the measurement. We see that theoretical tides and groundwater level contain significant peaks at both semidiurnal periods (solar semidiurnal period at 12.00 hours (S_2) and lunar semidiurnal period at 12.42 hrs (M_2)) and also the lunar diurnal period at 23.93 hrs (K_1) and solar diurnal period at 24.00 hours (S_1). Also several other peaks are contained in the groundwater level data around 26 and 27 hours, corresponding exactly to the peaks predicted by theoretical tides computation. Air pressure contains distinct period at 12.00 hours. This is, however, not caused by gravitational forces. It originates in the thermal changes of the atmosphere. It is also illustrated by the fact, that there is only one peak at 12:00 hours in the air pressure. If it was caused by gravitational forces, the lunar semidiurnal period would also be present at 12.42 hrs, see Lindzen and Chapman (1969). Diurnal periods are also not well pronounced in the air pressure data.

An insight into the harmonic components of the groundwater level is provided by the frequency-time analysis using the SVAL program – software developed for the analysis of seismic records, see Kolínský (2004 and 2010). It uses a traditional multiple-filtering technique (Dziewonski et al., 1969) with filtration in the frequency domain. This technique was modified and many new features and options were added (Kolínský and Brokešová, 2007). The method is implemented in software, which is universal in terms of use for analysis of any type of time series. Hence, it may be used to analyze seismic records as well as groundwater level data, acoustic signals and others.

The middle plot of Figure 6 shows a set of Gaussian filters weighting the spectrum of groundwater level data. Filters have constant relative resolution (Dziewonski et al., 1969), it means, the width of each filter is proportional to the central period of the filter – see the broadening of the filters toward longer periods in Figure 6. Multiplication of the spectrum by each filter produces a filtered spectrum, which is then transformed back to the time domain. Our method allows centering of the filters exactly to desired periods.

Figure 7 contains 21 harmonic components obtained by the filtering in the frequency domain. First eleven components (from 2 hours up to 25.82 hours) are presented in terms of their filters in the frequency domain in Figure 6. Left hand side labels of the Figure 7 show the vertical range of each harmonic component in millimeters. The raw record

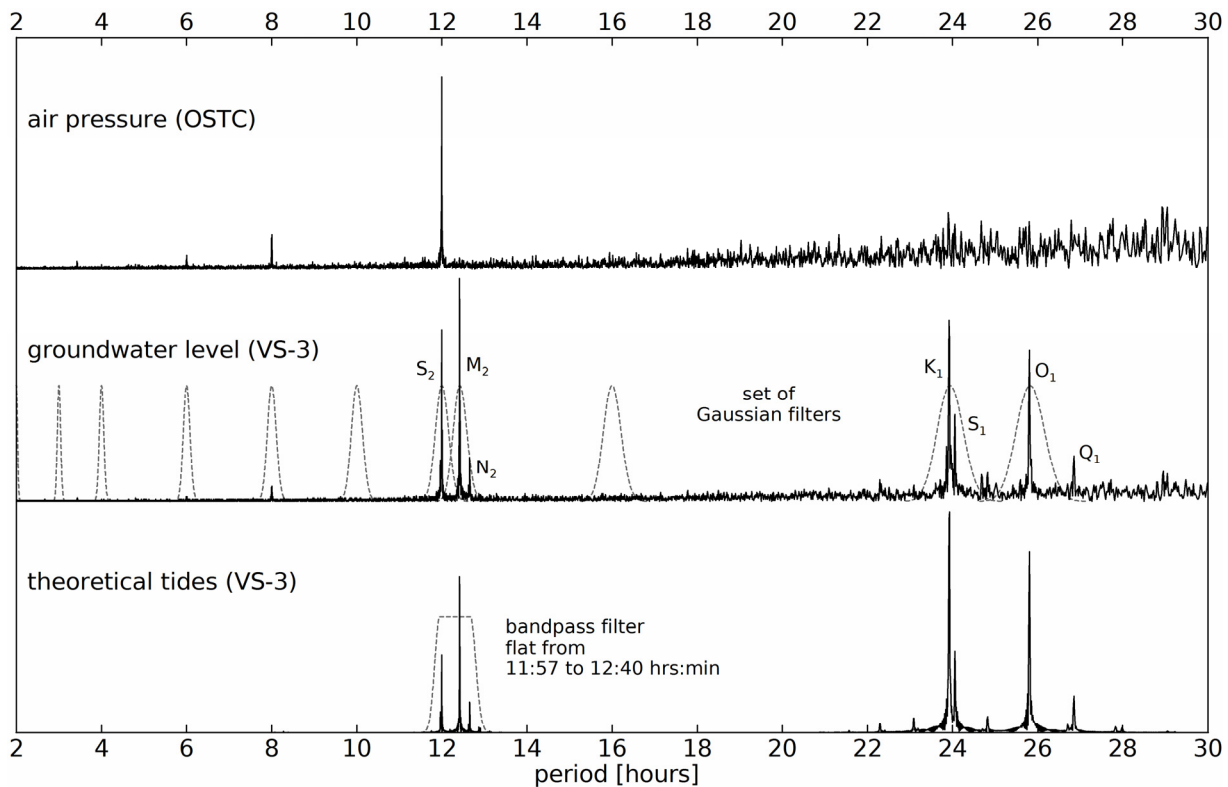


Fig. 6 Spectra of air pressure (OSTC), groundwater level (VS-3) and theoretical tides (VS-3) are shown. Notice the solar semidiurnal (around 12 hours) and solar and lunar diurnal (24 to 26 hours) peaks at all three quantities. However, the air pressure 12:00 hour peak is not caused by the gravitational tides but by the temperature changes. Lunar semidiurnal peak (12:25 hrs:min) is not visible in the air pressure data. In contrast to the theoretical tides, groundwater and air pressure contains also 6, 8 and 3 hours peaks in addition. Set of Gaussian filters, used for frequency-time analysis of groundwater level (Fig. 7) is shown in the middle plot and bandpass filter used for tidal and groundwater phase and amplitude analysis (Fig. 8) is shown in the bottom plot, both by dashed lines.

spans across 4 meters, its components range from 1.4 to 60 millimeters. Among the most pronounced components are: lunar (M_2) and solar (S_2) semidiurnal (12.00 and 12.42 hrs, vertical range of 16 mm), lunar diurnal (K_1) component (23.93 hrs, range 16 mm) and 4 and 7 days components (ranges 16 mm). The two highest harmonic components are fortnight (M_f) (13.66 days, range 24 mm) and monthly component (M_m) (27.56 days, range 60 mm). Longer periods are again smaller than the monthly one.

4.3. AMPLITUDES AND PHASES

To study the influence of the tides on the groundwater level, we compute the amplitude ratio and phase delay between these two quantities. The response of the rock massif to the tidal forces is delayed with respect to the tides and the aim of the analysis is to reveal, if the delay changes with time. The possible delay changes would indicate that stress conditions of the rock massif change with time. These changes are compared with the observed seismicity of the area. Because the periods of the highest tides are the two predominant semidiurnal lunar (M_2) and solar (S_2) components, we use these two for the analysis.

Groundwater data and modeled tidal data are processed by exactly the same manner and all parameters of the filtration are the same in both cases. The filtration is done in the same way as in case of the frequency-time analysis, however, the filter is not of a simple Gaussian shape centered at distinct period, but it is a bandpass filter with a portion of flat part in the middle.

The time series (real numbers of amplitude values) of groundwater level data and modeled tides with 10 min sampling interval are transformed to the spectral domain using FFT (see spectra of both quantities in Figure 6). The spectrum of each quantity is complex. Bandpass filter is applied to the complex spectrum of both quantities. The filter is flat between periods of 11:57 and 12:40 hrs:min and is effectively zero below the period of 11:37 and above the period of 13:00 hrs:min. Both sides of the filter are of the Gaussian shape as in the case of the multiple filtering analysis. Both filtered spectra are transformed back to the time domain using inverse FFT and a complex time series containing only the desired narrow period range are obtained.

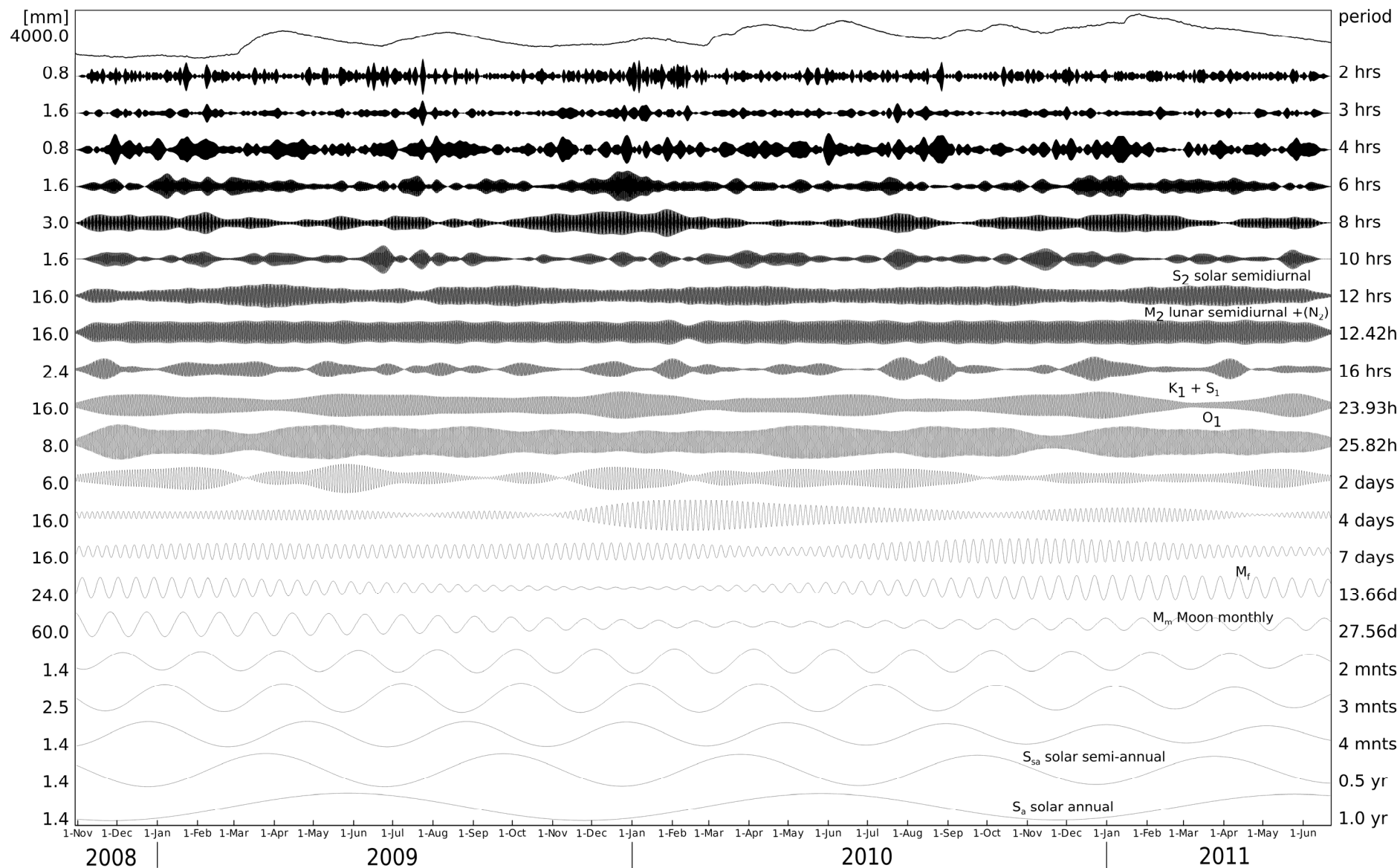


Fig. 7 Twenty one harmonic components of the VS-3 groundwater level data. Left hand side labels indicate the range of each trace in mm and right hand side labels show periods of the components. Raw measured data are in the uppermost trace. Compare the 4 meter range of the raw data with the ranges of harmonic components between 1.4 and 60 millimeters.

Up to this it resembles the previous frequency-time analysis. The difference is represented in the used filter – in the multiple filtering analysis, the filters have no flat part and are represented by pure Gaussian functions (Fig. 6, middle plot). In this bandpass filtering, both parts of the Gaussian function are separated by the flat part for which the spectrum is preserved (Fig. 6, bottom plot). The flat part is set so that the spectra contain both predominant semidiurnal periods. The filtration of each of the semidiurnal period separately is shown in Figure 7, traces of the period of 12.00 (S_2) and 12.42 (M_2) hrs, see previous section 4.2.

The real part of the bandpass filtered time series corresponds to the real values of filtered groundwater level and modeled tides. The imaginary part is a Hilbert transform of the real part and together they form an analytical signal. The modulus of the analytical signal is an envelope of the filtered time series. Both complex time series are divided. For each time, the complex filtered groundwater sample is divided by the complex filtered theoretical tidal sample. The ratio is again a complex time series. The modulus of the ratio represents the amplitude ratio between the groundwater and tides and the phase of the ratio represents the difference in their phases, e.g. the phase delay of the groundwater with respect to the tides. Since the amplitude ratio is computed using the complex time series (analytical signal), it represents the ratio of amplitudes of both quantities independently from the phase shift; in other words, it describes the amplitude response of the groundwater level to tides in terms of their envelopes and not the carrier signal itself.

Both the amplitude ratio and the phase delay are then smoothed with running average filter of 28 days length to avoid the fluctuation represented by the 14-days period. The results are given in Figure 8. Blue lines represent measured data, green lines are the filtered data and orange lines over the green ones are envelopes of the filtered data. This applies for all three wells as well as for the tidal potential theoretically computed for the VS-3 well. Filtered tides show clear interference of both semidiurnal periods (solar at 12.00 hrs and lunar at 12.42 hrs) which results in beats. An approximate period of the beats is 14 days and they are clearly marked by the orange envelope of the filtered data in Figure 8. Groundwater levels at the wells VS-3 and V-34 reflect the same pattern as tides, however, the tidal forcing on the HJ-2 well groundwater level is not so evident. Amplitude ratio between the groundwater level and its respective tide potential is shown by light blue line and the phase delay by the red line for all three wells. For simplicity, only the tidal potential for the VS-3 well is shown in the figure, however, for the computation, the respective tides were used for all three wells. The phase delays have the vertical axis in hours, the range is 6 hours and is the same for all three wells. The vertical amplitude scales of all other quantities for all

three wells (measured data, filtered data, envelopes and amplitude ratios) are also the same for comparison. In addition, we present a plot of average amplitudes computed from 1200 s long time windows for continuous OSTC seismic data by purple color in the bottom of Figure 8. This plot represents a seismic noise level at the station and period of year variations is clearly visible.

5. DISCUSSION

As it has been assumed, the earthquakes are located mainly close to the HPFZ, see Figure 3. However, some of them are found also in other parts of the area. The location error estimated using the four quarry blasts is less than 2 km outside the network. Assuming the fact that blasts are fired at the surface and so they can verify only shallower parts of the medium, we consider the error for the events C, D, F, H and K, which are out of the network, to be around 3 km. The network of four stations has been set up to cover the HPFZ and for the events A, B, E, G, J, L and M the location error is assumed to be smaller, around 1 km.

The error of the depths of the events is larger and since the expression for local magnitude estimation uses the hypocentral distance, the uncertain depth plays a role in the local magnitude estimation. Constant k_2 in the expression is set to join our local magnitude with the magnitude estimated by CRSN. For events B, E, F, and L, our local magnitudes give similar values as those from CRSN. However, event H has smaller magnitude in our study than the one estimated by CRSN. The difference may be caused by the larger error of its location. Event H lies outside of the network, and both its location and depth may have larger errors. The CRSN does not use stations CHVC and OSTC for the location and this may cause the discrepancy. Compared to the CRNS catalogue, in which only 6 events are presented, we found 12 events. Two of the events catalogued by the CRSN (August and December 2010) are re-determined to be quarry blasts.

Figure 4 allows to mutually compare groundwater levels of the three wells and also to compare them with the air pressure and precipitation data. We see similar level course of the wells VS-3 and V-34 from March 2010 to the July 2011. Both the shape and the amplitudes of the levels are similar. Both wells are deep and connected with the aquifers tapping similar geological layers. The HJ-2 well exhibits much different behavior: it is only a shallow well and thus local weather conditions play more important role. The course of the HJ-2 level is much more complicated – notice the high frequency disturbances.

Precipitation seems to have no influence on the two deep wells. On contrary to this, their influence on the shallow well is probable – see the abrupt variations during the whole monitoring time period at the HJ-2 level. However, to analyze the direct

connection quantitatively is not an objective of this paper.

By the analysis of 28-day interval around all twelve events, we do not find any rises or drops of groundwater levels. Figure 5 shows four local events (A, B – left top panel, M – right top panel and L – left bottom panel) as an example. Stejskal et al. (2009) proved pre-seismic groundwater level rises of +6 cm in case of the August 10, 2005, event and of +15 cm in case of October 25, 2005, event. Local magnitudes of these events were 2.4 and 3.3 and so they are bigger than the magnitudes detected in our study. In our study, the highest magnitude of 1.5 was reached for the event D, however, even for this event we do not find any steps even for the VS-3 well, where the steps were observed by Stejskal et al. (2009) for the two events in 2005. Event D is located 32.0 km SSW from the VS-3 well and this is two and three times farther than the events for which the steps were observed earlier: 16.8 and 11.3 km from VS-3 well, see Stejskal et al. (2009). The explanation for lack of any evidence of steps in the groundwater level can be, that in the period of interest, the earthquakes are too weak or too far from the wells.

An unusual drop of 95 cm is observed between 11:30 to 11:40, March 10, at the V-34 well, see right bottom panel in Fig. 5. This drop happened 18 hours before the great Tohoku M_w 9.0 earthquake, which occurred in Japan on March 11, 2011, at 05:46:24. This drop is preceded by an unusual rise of 19 cm between 01:20 and 01:30, March 10 (28 hours before the event). The strong groundwater level drop is also followed by another drop of 16 cm between 16:00 and 16:10 on March 11 (10 hours after the event). Even though we have a big gap in the V-34 well data, such a sequence of three steps within two days is very unusual in the 32 months monitoring period studied in our paper either, as it did not occur even in the years before (Stejskal et al., 2007 and 2009). Red dots in Fig. 8 give the times of the manipulation with the level loggers and data harvesting. There were no artificial influences on the level loggers in the time of the steps. Malfunction of the level logger is also improbable right at this time as it has been working for years without problems. We find it very unlikely that these steps would appear directly in the time of such unusually great earthquake by chance, however, we have no explanation for these steps. Furthermore, we also do not have any evidence, that these steps are directly connected with changes of stress conditions of the rock massif before the Tohoku earthquake.

Looking at shorter than semidiurnal periods in Figure 6 we see that tides reveal several peaks around 6:15 hrs:min and between 8:00 and 8:30 hrs:min, see Figure 9 where detailed spectra with log-scaled amplitudes are shown. The spectra are provided for tidal potential and strain, which both shows the peaks at the same periods and so only the tidal potential is shown in Figure 6. Shorter than 6:15 hrs:min periods are not contained in the tides at all. However, both

groundwater and air pressure contains distinct peaks exactly at 6 and 8 hours and also at 3:25 hours. This implies that also peaks in the air pressure spectrum for periods shorter than semidiurnal again originate in the thermal changes of the atmosphere and are not caused by the gravitational tides. The air pressure then influences the groundwater level which peaks exactly at the same periods.

Comparing Figures 6 and 9, we see that both the gravitational tides and the air pressure influences the groundwater levels, however, both these forces are independent. The groundwater level peaks at periods contained in the air pressure as well as in the gravitational tides, however, the air pressure does not peak at the gravitational periods. There is a coincidence of both thermal and gravitational effect at 12:00 hrs:min. At this period, both forces influence the groundwater level together, what is demonstrated by different ratios of S_2 and M_2 periods at the tidal and groundwater level spectrum, see Figure 6. If only the tides influence the groundwater, the amplitude of M_2/S_2 peak would be ~ 2 , as it is in the tidal spectrum. However, as the air pressure influences the groundwater level at S_2 and not at M_2 the ratio of M_2/S_2 amplitudes in the groundwater spectrum is much lower ($\sim 4/3$).

Figure 7 proves the predominant influence of the tides on the groundwater levels. Among the most dominant are both semidiurnal periods (12.00 and 12.42 hrs) and also the diurnal period (23.93 hours). The semidiurnal periods exhibit nearly constant course along the whole monitored time period – their amplitude does not contain any variations compared with the amplitudes of both shorter (10 hours) and longer (16 hours) periods. Stable shape and higher amplitudes of both semidiurnal periods compared to shorter and longer periods again proves that the tidal influence is much higher than the influences of other factors as the air pressure and precipitation. Then, fortnight (13.66 days) and monthly period (27.56 days) are the highest. Longer periods are again much smaller. Looking at the semi-annual and annual periods, we cannot distinguish if they are influenced by the tides or precipitation, since the precipitation period of one year length may cause the year variations of the water levels as well.

Figure 8 summarizes the groundwater levels and tide analysis. Interesting is the increased phase shift between the groundwater level and tides at the VS-3 well (from July 2009 to March 2010) which correlates with increased local seismic activity. However, our seismicity research started in the mid 2009 and so we have no evidence of the seismicity in the months before July 2009. But after the groundwater level of the VS-3 well went to its normal phase delay after the tides in February 2010, number of seismic events decreased. Unfortunately, the V-34 well has data gap directly in the period of the changed phase delay at the VS-3 well. However, the phase delay of both V-34 and HJ-2 wells is very complicated and does not

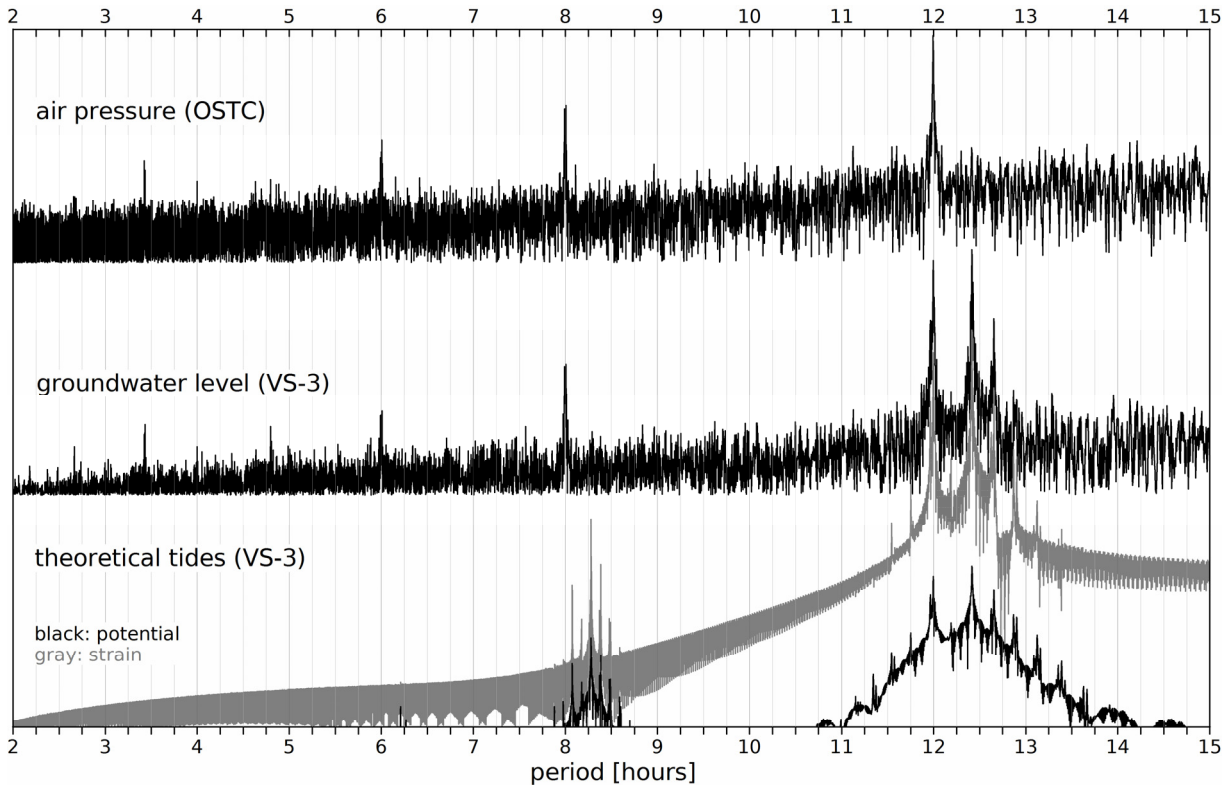


Fig. 9 Detailed spectra as in Figure 6. Amplitudes are in logarithmic scale and periods are presented only up to 15 hours. Grid lines drawn every 15 minutes allows to compare the position of particular peaks.

exhibit smooth constant course as the phase delay of the VS-3 well. Also the amplitude ratios show the same pattern: the VS-3 well has a constant amplitude ratio for all the time while both the V-34 and HJ-2 wells exhibit complicated behavior. This does not correspond to the fact that VS-3 and V-34 wells are both deep – their behavior is completely different in terms of amplitude ratio and phase delay with respect to tides.

Also note the previously discussed abrupt decrease in the groundwater level before the great Tohoku M_w 9.0 earthquake in the V-34 well in Figure 8.

Noise levels of the continuous OSTC seismic data shows clear year variations with the highest noise in the winter and lowest in the summer. This is probably caused by different weather conditions during the year.

6. CONCLUSION

Twelve earthquakes were found in the vicinity of the HPFZ using four seismic stations from July 2009 to April 2011. Their local magnitudes were estimated using a formula newly developed for this region. These magnitudes match well the magnitudes estimated by CRSN.

Groundwater levels in three wells were monitored from November 2008 to June 2011.

Frequency-time analysis allows to compare amplitudes and envelope shapes of different harmonic components of the water level courses. Each of the wells exhibits different behavior, however, filtration at the semidiurnal periods showed that all wells are sensitive to tidal forces. Both deep wells VS-3 and V-34 have similar water level courses, however, they exhibit different pattern of phase delay and amplitude response with respect to tides. Phase shift between the semidiurnal tidal forces and groundwater level response is reliably pronounced at the well VS-3. In the second half of 2009, it exhibits distinct change of the phase shift, which rises from 5 hours up to 8 hours and in the beginning of 2010 it again drops back to its original value. Most of the events detected in our study occurred from September 2009 to February 2010.

Mutual relationship among gravitational tides, air pressure and groundwater levels were studied. Groundwater levels are independently influenced by both gravitational tides and air pressure changes. Air pressure changes are caused by thermal tides of the atmosphere.

The correlation between seismic events and groundwater level changes is very complex and currently there is no comprehensive explanation of their relation. We see that the VS-3 well may be sensitive to the local seismic activity (increased phase shift at the VS-3 well corresponding to the period of

increased local seismic activity). However, we have no evidence for any causality between the two observed phenomena. No distinct water level steps were found in connection with local seismic events.

ACKNOWLEDGEMENTS

This research was supported by the Grant No. 205/09/1244 of the Czech Science Foundation and by the Institute's Research Plan No. A VOZ30460519. It was also financed by the CzechGeo/EPOS project. Data from two of the stations used in this study were kindly provided by Jan Zedník of the Czech Regional Seismic Network, Institute of Geophysics, Academy of Sciences of the Czech Republic, v.v.i. Part of the groundwater data from the VS-3 well was provided by Jan Kašpárek, T. G. Masaryk Water Research Institute, v.v.i. We are grateful to Lumír Skalský not only for his theoretical tide models, but also for discussion of the issues concerning the Earth tides and related phenomena.

REFERENCES

- Brož, M. and Štrunc, J.: 2011, A new generation of multichannel seismic apparatus and its practical application in standalone and array monitoring, *Acta Geodyn. Geomater.*, 8, No. 3 (163), 345–352.
- Cháb, J., Stráňík, Z. and Eliáš, M.: 2007, Geological map of the Czech Republic 1:500000, Czech Geological Survey.
- Dehant, V.: 1987, Tidal parameters for an inelastic Earth, *Physics of the Earth and Planetary Interiors*, 49, 97–116.
- Dziewonski, A., Bloch, S. and Landisman, M.: 1969, A technique for the analysis of transient seismic signals, *Bull. Seism. Soc. Am.*, 59, 427–444.
- Fischer, T., Horálek, J., Michálek, J. and Boušková, A.: 2010, The 2008 West Bohemia earthquake swarm in the light of the WEBNET network, *Journal of Seismology*, 14, 665–682.
- Gaždová, R., Novotný, O., Málek, J., Valenta, J., Brož, M. and Kolínský, P.: 2011, Groundwater level variations in the seismically active region of Western Bohemia in the years 2005–2010, *Acta Geodyn. Geomater.*, 8, No. 1 (161), 17–27.
- Jakobsdóttir, S.S., Guðmundsson, G.B. and Stefánsson R.: 2002, Seismicity in Iceland 1991–2000 monitored by the SIL seismic system, *Jökull*, 51, 87–94.
- Kolínský, P.: 2010, Surface wave analysis and inversion – application to the Bohemian Massif, PhD thesis, Department of Geophysics, Faculty of Mathematics and Physics, Charles University, Prague.
- Kolínský, P. and Brokešová, J.: 2007, The Western Bohemia uppermost crust shear wave velocities from Love wave dispersion, *Journal of Seismology*, 11, 101–120.
- Kolínský, P.: 2004, Surface wave dispersion curves of Eurasian earthquakes: the SVAL program, *Acta Geodyn. Geomater.*, 1, No. 2 (134), 165–185.
- Lindzen, R.S. and Chapman, S.: 1969, Atmospheric tides, *Space Science Reviews*, 10, No. 1, 3–188.
- Málek, J., Brož, M., Stejskal, V. and Štrunc, J.: 2008, Local seismicity at the Hronov-Poříčí Fault (Eastern Bohemia), *Acta Geodyn. Geomater.*, 5, No. 2 (150), 171–175.
- Schenk, V., Schenková, Z. and Pospíšil, L.: 1989, Fault system dynamics and seismic activity - examples from the Bohemian Massif and the Western Carpathians, *Geophysical Transactions*, 35, 101–116.
- Skalský, L.: 1991, Calculation of theoretical values of the tidal strain components with respect to their practical use, *Proceedings from seminary "Advances in gravimetry"*, December 10 - 14, 1990, Smolenice, 179–184, Geophysical institute, Slovak Academy of Sciences, Bratislava.
- Špaček, P., Sýkorová, Z., Pazdírková, J., Švancara, J. and Havíř, J.: 2006, Present-day seismicity of the south-eastern Elbe Fault System (NE Bohemian Massif), *Stud. Geophys. Geod.*, 50, 233–258.
- Stefánsson, R., Bödvarsson, R., Slunga, R., Einarsson, P., Jakobsdóttir, S.S., Bungum, H., Gregersen, S., Havskov, J., Hjelme, J. and Korhonen, H.: 1993, Earthquake prediction research in the South Iceland Seismic Zone and the SIL project, *Bull. Seism. Soc. Am.*, 83(3), 696–716.
- Stejskal, V., Kašpárek, L., Kopylova, G.N., Lyubushin, A.A. and Skalský, L.: 2009, Precursory groundwater level changes in the period of activation of the weak intraplate seismic activity on the NE margin of the Bohemian Massif (Central Europe) in 2005, *Stud. Geophys. Geod.*, 53, 215–238.
- Stejskal, V., Skalský, L. and Kašpárek, L.: 2007, Results of two-years seismo-hydrological monitoring in the area of the Hronov-Poříčí Fault Zone, Western Sudetes, *Acta Geodyn. Geomater.*, 4, No. 4 (148), 59–76.
- Stejskal, V., Štěpančíková, P. and Vilímek, V.: 2006, Selected geomorphological methods assessing neotectonic evolution of the seismoactive Hronov-Poříčí Fault Zone, *Geomorphologica Slovaca*, 6 (1), 14–22.
- Valenta, J., Stejskal, V. and Štěpančíková, P.: 2008, Tectonic pattern of the Hronov-Poříčí Trough as seen from pole-dipole geoelectrical measurements, *Acta Geodyn. Geomater.*, 5, No. 2, 185–195.
- Wahr, J.M.: 1981, Body tides on an elliptical, rotating, elastic and oceanless earth, *Geophysical Journal of the Royal astronomical Society*, 64, 677–703.
- Wenzel, H.-G.: 1993, Earth tide data processing package ETERNA, version 3.0. Program manual, Status August 1st, 1993, Geodätisches Institut, Englerstr. 7, D-76128 Karlsruhe 1.
- Woldřich, J.N.: 1901, Earthquake in the north-eastern Bohemia on January 10, 1901, *Transactions of the Czech Academy of Sciences, Series II*, 10(25), 1–33, (in Czech).
- Zedník, J. and Pazdírková, J.: 2010, Seismic activity in the Czech Republic in 2008. *Stud. Geophys. Geod.*, 54, 333–338.
- Zschau, J. and Wang, R.: 1981, Imperfect elasticity in the Earth's mantle. Implications for Earth tides and long period deformations, *Proceedings of the 9th International Symposium on Earth Tides*, New York 1987, 605–629, editor Kuo, J.T., Schweizerbart'sche Verlagsbuchhandlung, Stuttgart.

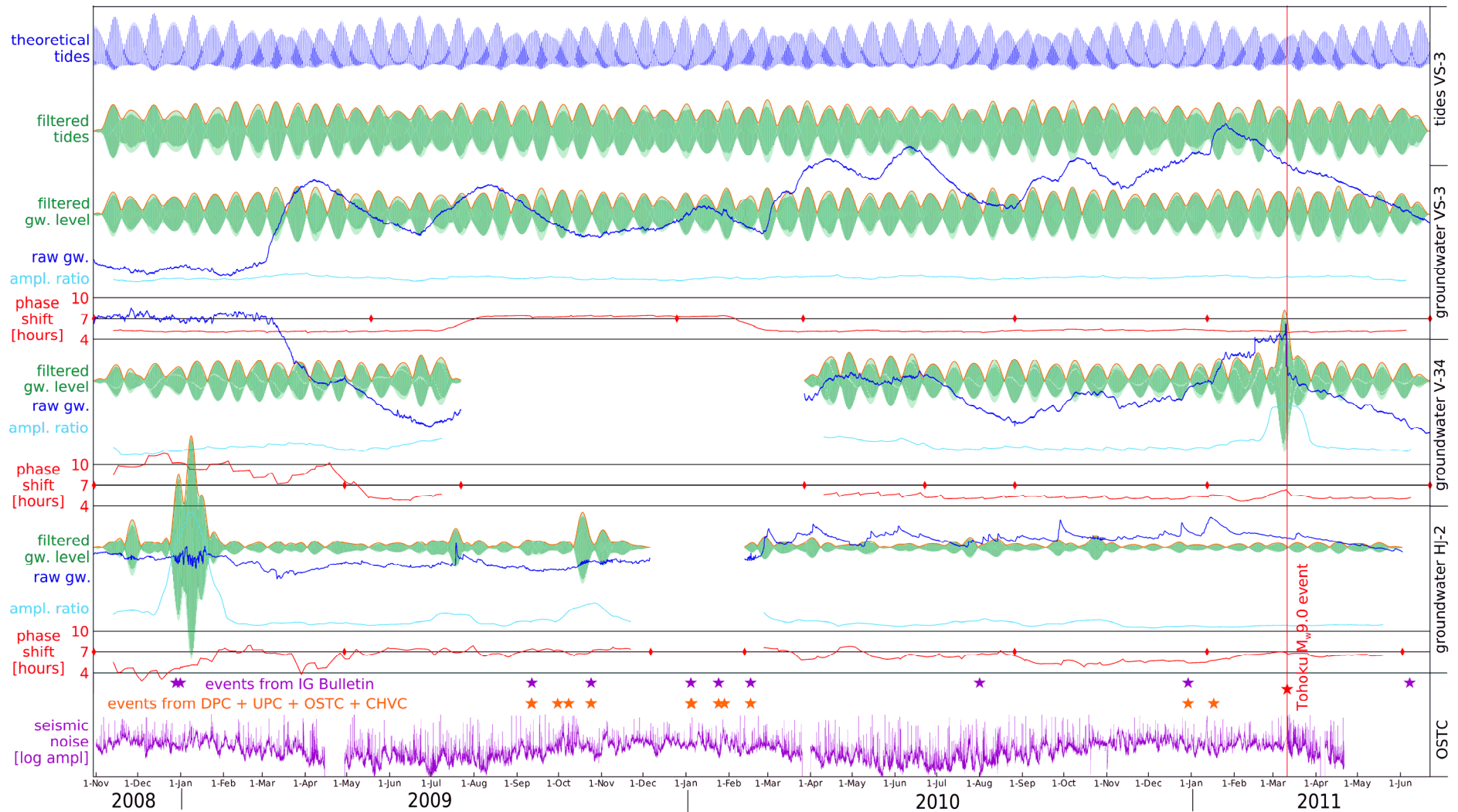


Fig. 8 Raw and filtered groundwater level data are shown for all three wells. For the station VS-3 (Adršpach), also theoretical modeled tides are presented. Following line types are used for all four time series: blue line: measured or modeled data; green line: data filtered between 11:57 and 12:40 hrs:min; orange line contouring the green data: envelopes of filtered time series. Red dots indicate times of data downloading. Amplitude ratios between filtered groundwater level and filtered theoretical tides are shown in light blue; the phase shifts between the two are shown in red (hours) for all three wells. Purple stars are events from the Seismic Bulletin of the Geophysical Institute AVCR and orange stars are the events detected in our study using four local stations. The origin time of the Great Tohoku earthquake, March 11, 2011, is also depicted. Vertical scales for the same quantities (measured data, filtered data, amplitude ratios and phase shifts) are the same for all three wells. The bottom plot purple curve shows average of amplitudes in 1200 seconds window for the vertical component (Z) of continuous seismic records from the OSTC station.